Surface acoustic wave devices with graphene interdigitated transducers

Jian Zhou[1,a)], Xianglong Shi[2,a)], Dingbang Xiao[1,*], Xuezhong Wu[1], Jiangpo Zheng[3], Jikui Luo[4], Ming Zhuo[1], Xiang Tao[5], Hao Jin[5], Shurong Dong[5], Ran Tao[6], Huigao Duan[3,*], YongQing Fu[6,*]

[1]College of intelligent science and engineering, National University of Defense Technology, 410073, Changsha, P. R. China
[2] Beijing Aerospace Micro-electronics technology Co., 100854, Beijing, P. R. China
[3]College of Mechanical and Vehicle Engineering, Hunan University, Changsha 410082, P. R. China
[4]Institute of Renewable Energy and Environmental Technologies, Bolton University, Bolton BL3 5AB, United Kingdom
[5]Department of Information Science and Electronic Engineering, Zhejiang University, Hangzhou 310027, P. R. China
[6]Faculty of Engineering and Environment, Northumbria University, Newcastle upon Tyne, NE1 8ST, UK.

a) The same contribution
*E-mail: dingbangxiao@nudt.edu.cn, duanhg@hnu.edu.cn, richard.fu@northumbria.ac.uk

Abstract

This paper reports the development of high performance surface acoustic wave (SAW) devices by using graphene as a virtually massless interdigital transducer (IDT) to mitigate mass-loading effects. Different layers of graphene electrodes were made and their influences on the SAW device performance were experimentally and theoretically evaluated. Results showed that 4-layer graphene with a value of sheet resistance less than 77.6 Ω/sq. and graphene IDTs of at least 80 pairs are needed to obtain the optimum performance of graphene IDT SAW devices. Furthermore, the optimal ratio of aperture/wavelength for the graphene IDT electrode was found to be 5. Graphene based SAW devices, with a resonance frequency of 154 MHz, transmission signal amplitude of 30 dB and K^2 of 3.78%, were fabricated and successfully demonstrated for applications in breathing monitoring.

Keywords: SAW, graphene IDTs, sheet resistance, geometry effects, sensors

1. Introduction

Surface acoustic wave (SAW) resonators are one of the building blocks for electronics with wide-range applications in communication systems (e.g. filters, duplexers etc.) [1, 2], sensors for temperature, humidity, pressure, strain, gas, DNA, protein etc., acoustofluidics and lab-on-a-chip[3-7]. Conventional SAW devices are typically made on piezoelectric bulk materials or piezoelectric thin films, consisting of metallic (such as Au or Pt) interdigitated electrodes (IDTs) with a thickness in the range of tens to hundreds of nanometers[8, 9]. Such thick metallic IDTs will reduce operation frequencies of the SAW devices and magnitudes of the generated acoustic signals [10], thus they may not be suitable for high frequency applications. The "heavy and thick" metal fingers will also reflect the mechanical waves and induce secondary effects such as the generations of triple transit signals and bulk acoustic waves[11]. Several methods have been established to minimize these secondary effects induced by the metallic IDTs. For instance, metals with a relatively low density such as Al are often embedded into the substrate to reduce undesirable reflections[12] for high frequency SAW devices. Another approach is that the geometry of the IDT fingers is designed to reduce destructive interferences of the acoustic waves reflected at successive fingers, such as split fingers or single-phase unidirectional transducers[7], which normally require more than two fingers per SAW wavelength or a precise control of the finger width and separation.

Graphene, being the thinnest and lightest, yet the strongest material that can be processed by photolithography[13], is expected to mitigate the mass-loading effect and reduce the secondary effects caused by the mass loading of electrodes when they are used as the IDTs[14]. Leong et al.[11] carried out theoretical analysis using a finite element method to investigate the mitigation of the secondary effects, and results showed that unlike metal electrodes, graphene electrode has the least triple transit signal and bulk acoustic wave generations compared with Al and Au-Cr electrodes. We have previously reported the transparent SAW resonators using graphene IDTs as the conductive electrodes[15], showing that the graphene electrode can be used to fabricate transparent SAW devices with reasonable performance.

However, there is lack of a systematic exploration of using the graphene as the virtually massless IDTs for SAW devices compared with the metallic electrodes. It is unclear how the graphene electrodes would affect the performance of SAWs; and how many layers of graphene and how low the series resistance of the graphene electrode are needed to achieve reasonable performance SAW devices; as well as how to optimize the geometric structures to achieve a better performance of graphene SAW devices.

This paper reports a systematic investigation on the influences of material/structure properties (i.e., number of layers and sheet resistance) and geometry of graphene on the SAW resonator performance. Graphene based SAW devices show that the graphene IDT electrodes are virtually massless compared with metallic electrodes, and they have high performance and can be used for sensing applications, e.g. to monitor respiration. The paper will also show the comparison performance of SAW devices with graphene and metal electrodes.

2. Experimental

Figure 1 shows a schematic drawing of fabrication process of the SAW device on $LiNbO_3$ substrates with graphene IDTs. The process is listed as follows: 1) A 128° Y-X one-side polished single-crystal $LiNbO_3$ wafer was used as the substrate; 2) Cr/Au(5nm/100nm) wire pad was patterned using sputtering, photolithography and etching process (e.g., a standard traditional SAW fabrication process based on lift-off); 3) The CVD graphene (supplied by XFNANO Inc.) was then transferred onto the $LiNbO_3$ substrate (Figure 2 shows CVD graphene transfer process); 4) A layer of AZ1500 photoresist was spun onto the $LiNbO_3$ substrate at 4000 rpm for 40 s and baked at 100 °C (60 s), with UV exposure (90 mW/cm^2), and development for 60 s in AZ300MIF (2.38%); 5) The graphene IDT was patterned subsequently by etching using an oxygen plasma (with the O_2 of 30 sccm, pressure of 1 Pa, power of 50 W and time of 60 s); 6) The photoresist on the graphene IDT was removed by immersing the sample in acetone and subsequent cleaning in isopropyl alcohol and deionized water. Finally, the graphene IDTs with Cr/Au wire pad for SAW devices were achieved.

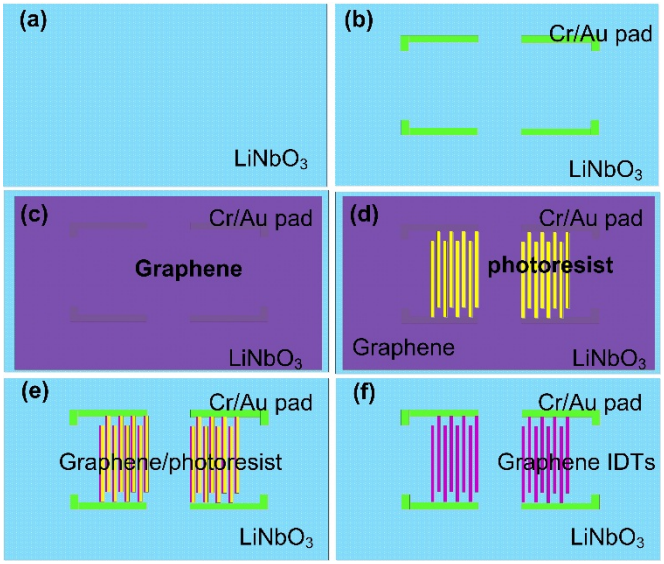

Figure 1. Schematic drawing of fabrication process of the SAW device on $LiNbO_3$ substrates with graphene IDTs: (a) Preparing the $LiNbO_3$ substrate; (b) Patterning the Cr/Au wire pad; (c) Transferring graphene onto the substrate; (d) Photolithography process; (e) Etching the graphene; (f) Removing the photoresist to form graphene IDTs.

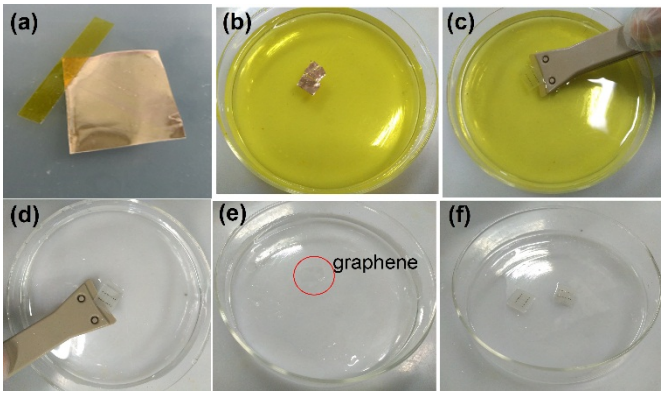

Figure 2. Process of the transfer process of CVD graphene on the target substrate: (a) Monolayer CVD graphene on copper substrates was bought from the XFNANO Inc. (Nanjing, China); (b) The copper foil was etched in a bath filled with copper etchant; (c)&(d) The graphene film was transferred from the copper etchant to the deionized water; (e)The graphene film was rinsed with deionized water to remove residual etchant and this step was repeated for three times. (f) The graphene film was transferred to the flat target surface, and then air-dried. By repeating these steps on the same substrate, multilayered graphene films can be prepared.

The graphene IDTs with Cr/Au wire pads for SAW devices were realized as shown in Fig. 3(a). As the graphene is transparent on the $LiNbO_3$ substrate, the graphene layer cannot be easily identified because of no apparent contrast

(Fig. 3(a)). The fabricated graphene-Au/ $LiNbO_3$ SAW devices can be observed using the Scanning Electron Microscope (SEM) as shown in Figs. 3(b) and 3(c), confirming the existence of the graphene IDTs. Figure 3(d) shows the morphology and surface roughness of the surface of graphene IDTs measured using an atomic force microscope (AFM), and the root mean square (RMS) roughness of the graphene film is less than 1 nm over a large area of 4×4 μm^2.

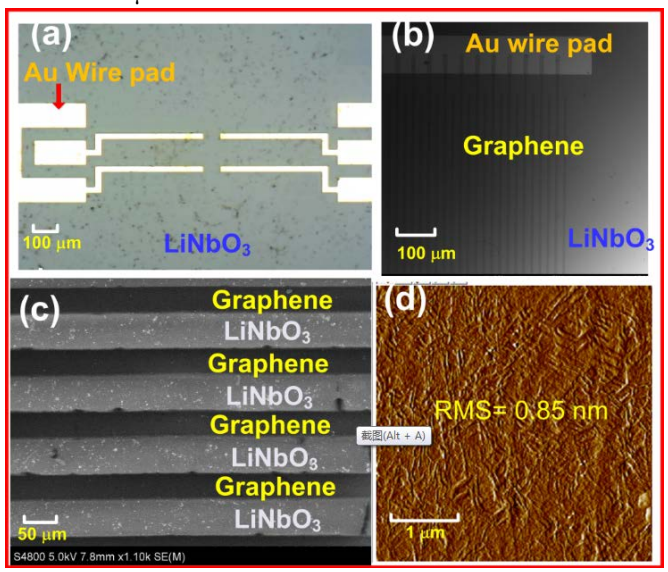

Figure 3. (a) microscopic images of graphene-Au/$LiNbO_3$ and Al/$LiNbO_3$ SAW devices; (b) &(c) SEM images of the fabricated graphene-Au/ $LiNbO_3$ SAW device; (d) AFM image of film surface of graphene IDTs.

To study the effects of graphene layers and series resistance of the graphene electrode on the performance of SAW devices, graphene-Au/$LiNbO_3$ SAW devices with 1, 2, 3, 4 layered graphene (showing the different sheet resistance) as IDTs have been fabricated and tested. Also SAW devices with different IDT finger pairs (N) (10~100) and different ratios of aperture/wavelength (w/λ, 2.5~40) were fabricated and tested. The whole length of SAW device (including the wire pad and IDT length) is about 10 mm for wavelength of 40 μm and 6 mm for wavelength of 24 μm, with the IDT pairs of 100.

3. Results and discussion

Crystal quality of the layer by layer stacked graphene films was analyzed using the Raman spectroscopy and the results are shown in Fig. 4(a). It can be observed that the peak position values are at about 1580cm^{-1} and 2700 cm^{-1} for all the layers of graphene films, corresponding G-band frequency and 2D band frequency.[16] As the graphene layers were transferred one after another, the intensity ratios of I_{2D}/I_G are 1.39, 1.22, 1.08 and 0.74, respectively, decreasing with the increase in the layers, which is consistent with those from the literature[17]. Shen etc. [18]showed that the Raman intensity of G band should be proportional to the thickness of graphene samples (from 1 to 4 layers), by considering the multiple reflection of Raman signal inside the graphene layer as well as the interference effect due to the multiple reflection of the incident laser, thus mainly contribute to the decrease of intensity ratios of I_{2D}/I_G.

The transmission (S_{21}) characteristics of the graphene based SAW devices were measured using an Agilent E5071C network analyzer. The results are shown in Fig. 4(b) and also summarized in Table 1. Apart from the SAW device with 1-layer graphene IDT which has no obvious signal, all the other devices show the resonance characteristics. The resonant frequency, f_0, is about 91.7 MHz with the wavelength of 40 μm, revealing the typical $LiNbO_3$ Rayleigh mode. The amplitudes of transmission signals S_{21} of the SAW devices are 0, -37, -32, -26 dB, respectively, increasing with increase in graphene layers and a large signal amplitude up to about 20 dB is obtained from the device with 4-layer graphene IDTs. The results show that thicker graphene IDT electrodes will improve the performance of the SAW devices.

To theoretically analyze the numbers of graphene layers on the performance of graphene/$LiNbO_3$ SAW device, finite element model /boundary element model (FEM/BEM) method was used to analyze the generalized periodic array. The two-dimensional numerical models for the simulation of a periodic array of graphene electrodes on a semi-infinite half space were analyzed. The graphene is a thin atomic layer and the $LiNbO_3$ is taken as an isotropic half space. The Green's function for a semi-infinite piezoelectric substrate was firstly employed, where only charges at the electrode/substrate interface (z=0) were considered[19]. The Green's function is linked with particle displacements u and electric potential φ with mechanical stress components in z-direction t and charges σ at the interface based on the following equations:

$$\begin{pmatrix} u(x) \\ \varphi(x) \end{pmatrix} = \sum_{j=1}^{N_e} \int_{c_j-a_j}^{c_j+a_j} G_\gamma^p(x-x') \begin{pmatrix} t_s(x') \\ \sigma(x') \end{pmatrix} dx' \quad (1)$$

here N_e is the number of electrodes for one period of the array, c_j is the x coordinate of the electrode center, and a_j is the half electrode width for the j^{th} electrode of the elementary period. $G_\gamma^p(x)$ is the periodic harmonic Greens function (which was first introduced by Plessky *et al.[20]*.

The second simulation step was to integrate the electrode's mechanical behavior into the system. Using a similar approach as described in Ref [20], we assumed the metallic electrodes are homogeneous, isotropic, and elastic (ρ is the mass density; λ and μ are the Lame constants). Each electrode was discretized into triangular finite elements (linear or quadratic interpolation can be used) and the FEM was used to derive linear equations relating to the nodal displacement and force vectors (**U**, **F**):

$$(\mathrm{K}-\omega^2\mathrm{M})\mathrm{U}=\mathrm{F} \quad (2)$$

where **K**, **M** are stiffness and mass matrix, respectively, and **F** is computed from stresses **t***s* according to:

$$F_i=\int_{\Gamma_{es}} t_s(x)W_i(x)dx \quad (3)$$

Wi(*x*) is the FEM basis function associated with node *i*. The derivation process of the formula and calculation method was described in details in the supplementary materials. Finally, the current flowing into the *j*-finger can be calculated by the following equation:

$$I_j=\int_{-a_j}^{a_j}\frac{\partial\sigma(x)}{\partial x}dx \quad (4)$$

Once the current flowing into every single finger was obtained, we could then calculate the admittance matrix of the SAW with arbitrary number of electric ports according to the circuit theory. Based on this, the scattering matrix and the frequency response would be obtained.

With the increase in layers of the graphene film, the sheet resistance of the graphene layer was measured to be 250, 130.5, 84.6, 77.8 Ω/sq. respectively. Fig. 4(c) shows the effects of sheet resistance of IDTs on the transmission signals of SAW devices using the theoretical calculation by FEM/BEM model and the results show that with the decrease in the sheet resistance, the transmission signals become more closely agreed with the experimental results. The thicker the graphene film is, the lower the sheet resistance, thus leading to a better SAW performance. It is also clear that when the sheet resistance of the graphene layer is larger than the 77.8 Ω/sq, the SAW performance is poor, implying that the sheet resistance of the graphene electrode layer should be at least smaller than 77.8 Ω/sq for the SAW devices.

The electromechanical coupling coefficient (K^2) of a SAW device can be evaluated by[21]

$$K^2=\pi G_m(f_0)/4NB_s(f_0) \quad (5)$$

where N is the finger pairs, G_m (f_0) and B_s (f_0) are the motional conductance and static susceptance of the input port at f_0, respectively. The measured K^2 values are increased from 0%, 1.5 %, 2.0%, 2.7 %, as the graphene layers are increased from 1 to 4. As 4 layers of graphene have the lowest sheet resistance, hence also the best SAW performance, we chose 4-layer graphene as the SAW IDTs to investigate the geometric effects of graphene IDTs on the performance of SAW devices.

Table 1 Effect of layers of graphene on the characteristics of graphene-Au/LiNbO$_3$ SAW devices.

sample no.	λ (μm)	Graphene layers	Sheet resistance (Ω/□)	transmittance	f_0 (MHz)	Signal amplitude (dB)	K^2 (%)
A1	40	1	250	97.69%	/	/	/
A2	40	2	130.5	95.51%	91.64	8	1.5%
A3	40	3	84.6	92.41%	91.67	13	2.0%
A4	40	4	77.8	90.09%	91.72	20	2.7%

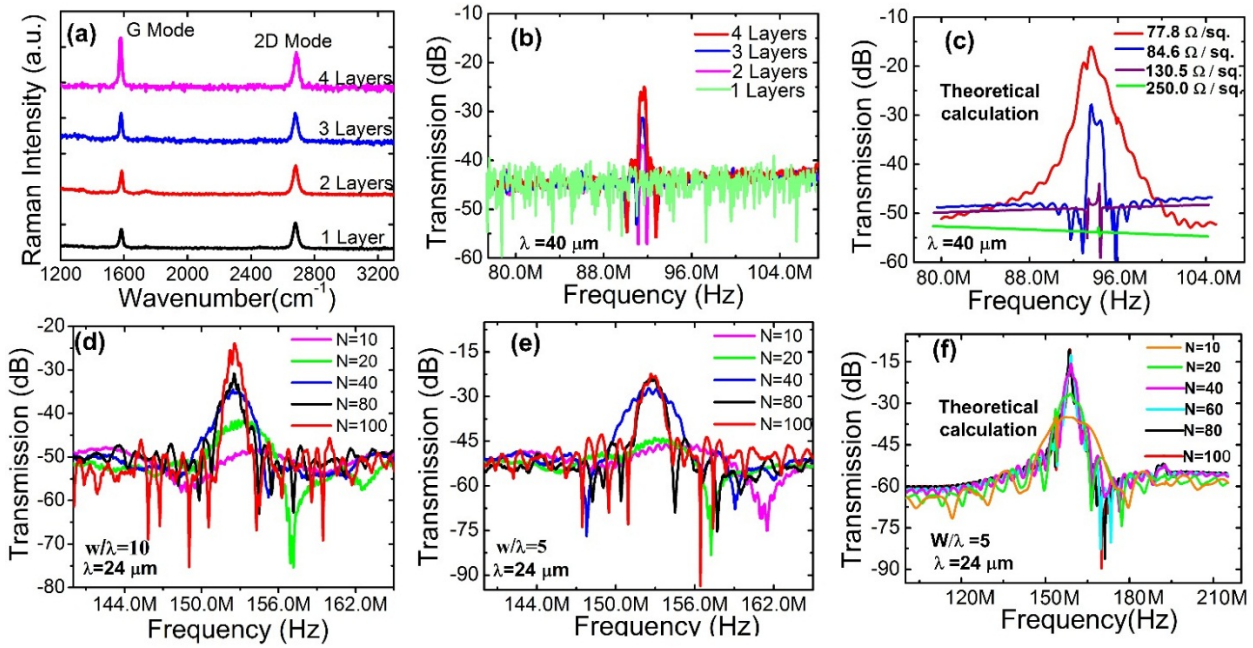

Figure 4. (a) Raman spectra of the graphene films as a function of graphene layers; (b) Transmission characteristics of the graphene IDT SAW devices with different layered graphene IDTs; (c) Theoretical S_{21} characteristics of the graphene IDT SAW devices with different graphene sheet resistances; (d) &(e) S_{21} characteristics of the graphene IDT SAW devices with different IDT pairs; (f) Theoretical S_{21} characteristics of the graphene IDT SAW devices with different IDT pairs.

The effect of N on the SAW characteristics has been studied for the devices with the same wavelength of 24 μm at the different ratios of aperture/wavelength (w/λ). Results show that when the N is increased from 10 to 100 pairs, the amplitude of the transmission signal increases as shown in Fig. 4(d) and 4(e). With the increase in the N, the excitation efficiency of SAW devices increases, thus leading to the larger signal amplitude of S_{21}[22]. On the other hand, when the IDT pairs are larger than 80 (e.g. 100), the devices do not show apparent differences, implying that 80 pairs of IDTs are enough for the graphene based SAW devices. This is because when the N exceeds about 80, the losses associated with scattering from the electrodes begin to neutralize any additional advantage associated with the increased number of electrodes[23]. The experimental results are in good agreement with the theoretical calculation as shown in Fig. 4(f).

Figure 5 present the effect of the aperture/wavelength ratio on the performance of the graphene based SAW devices. The wavelengths of the device are 24 μm and 40 μm, while the ratio of aperture/wavelength is varied at 2.5, 5, 10, 20 and 40. It can be seen that when the value of the ratio of aperture/wavelength is increased from 2.5 to 5, the amplitude of the transmission signal of graphene based SAW devices is increased. However, the amplitude of the transmission signal gradually becomes decreased significantly when the value of the aperture/wavelength is increased to 40. The optimal value was found to be 5 for the graphene based SAW device: with a resonance frequency of 154 MHz, transmission signal amplitude of 30 dB, and a K^2 value of 3.78%, at IDT pairs of 80, the wavelength of 24 μm and w/λ of 5. The devices with other wavelengths shows the same trend as shown in Fig.5(d).

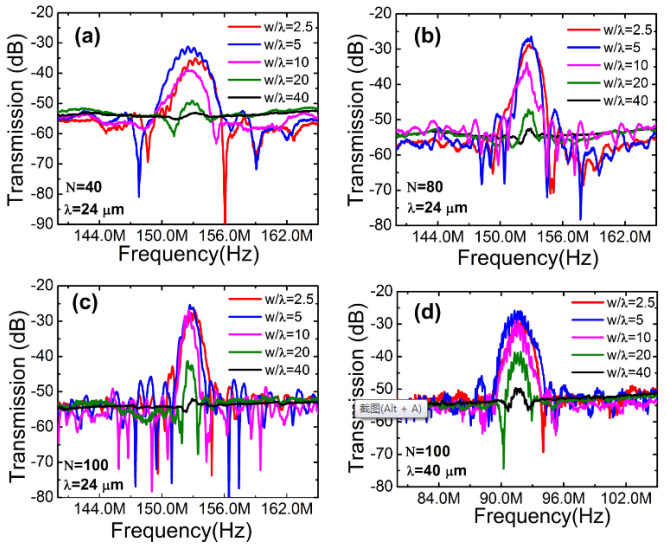

Figure 5. Effect of aperture/wavelength of graphene IDT on the S_{21} characteristics of the graphene IDT SAW devices at: (a) λ of 24 μm, graphene IDT pairs of 40; (b) λ of 24 μm, graphene IDT pairs of 80; (c) λ of 24 μm, graphene IDT pairs of 100; (d) λ of 40 μm, graphene IDT pairs of 100;

The existence of the optimal value of aperture/wavelength is because when the aperture/wavelength is too small, such as at 2.5, the aperture of the IDT is relatively too short, and the IDTs cannot generate strong acoustic wave and signals. The transmission signal will increase with the increase of aperture/wavelength. However, when the value of aperture/wavelength exceeds 5, the longer apertures will lead to the increase of the resistance of the IDT, resulting in poor resonance signals.

The metal electrode (Cr/Au) SAW devices with different values of aperture/wavelength were also fabricated for comparison, with the results shown in Fig. 6. With the increase in aperture/wavelength ratio from 5 to 40, the S_{21} amplitude begins to increase and gradually becomes saturated. The reason is that the sheet resistance of metal electrodes is quite low (less 10 Ω/sq.), and simply increasing aperture/wavelength (IDT length) will not lead to much increased resistance of IDTs. Therefore, when the aperture/wavelength is increased from 5 to 40, S_{21} amplitude will not decrease, significantly different compared to that of graphene based SAW devices.

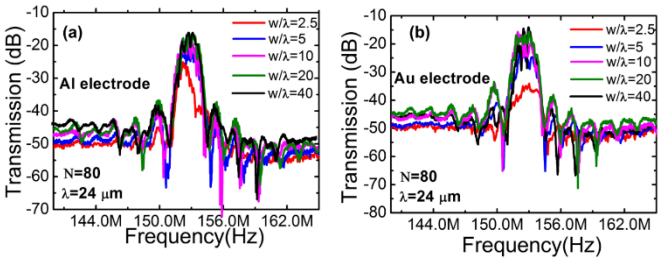

Figure 6. Effect of aperture/wavelength on the S_{21} characteristics of the (a) Al/$LiNbO_3$ and (b) Au/$LiNbO_3$ SAW devices, at IDT pairs of 80, the λ of 24 μm.

Figure 7 are the comparisons of S_{21} characteristics of SAW devices with graphene, Al and Au IDTs respectively. It is clear that in the low frequency range, all the peaks are related to the Rayleigh mode, and the resonance frequencies (~154 MHz) for the SAW with different IDTs are similar and do not show apparent differences. However, in the high frequency (5^{th} order Rayleigh mode), the graphene electrode shows much higher resonant frequencies and better performance than those of the metal IDTs. This is because the graphene is the thinnest and lightest conductive material

and does not introduce significant mass loading effect, thus it shows that graphene-IDT SAW devices are good for high frequency applications.

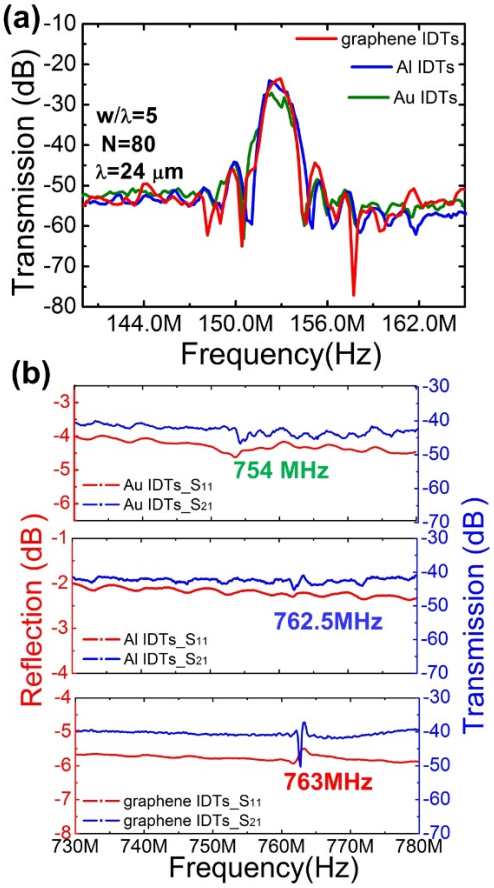

Figure 7. Comparison of S_{21} characteristics of SAW devices with graphene, Al and Au IDTs. All the devices have 80 pairs of IDTs, the 24 μm wavelength and 5 w/λ ratio. (a) Rayleigh mode, (b) 5th-order Rayleigh mode;

Figure 8 are the comparisons of S_{21} characteristics of SAW devices with graphene, thick Au IDTs and 30nm Au IDTs respectively. It is clear that, with the Au thickness decrease, the SAW performance become worse due to larger sheet resistance of thin metal electrode. The SAW performance with 2nm graphene IDTs is better than the SAW performance with 30 nm Au electrode.

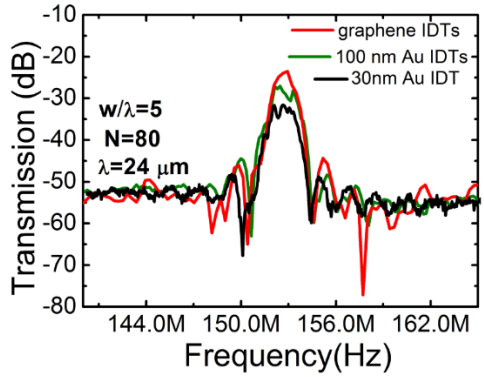

Figure 8 Comparison of S_{21} characteristics of SAW devices with graphene, Au IDTs. All the devices have 80 pairs of IDTs, the 24 μm wavelength and 5 w/λ ratio.

To verify the graphene based SAW application, we have conducted a demonstration of human breathing detection using the fabricated SAW devices. The monitoring of the human breath and other gas molecules emanating from the human body and from the environment around the human body is expected to play an important role in personalized medicine, healthcare and human motion[24]. Figure 9 show the resonant frequencies of the transparent SAW sensors placed on the upper lip under discontinuous respirations as a function of time. The resonant frequency of the sensor shifts downwards when it receives expiratory air due to the changes in the humidity (as temperature change is less than 3°C), and the sensor recovers to its original value when the volunteer inhales. The volunteer's normal respiratory rate detected by our graphene SAW sensor is about 18 min^{-1}, which is within the range of respiratory rates of a healthy adult. The results are consistent with other SAW sensors based on metal electrode[25].

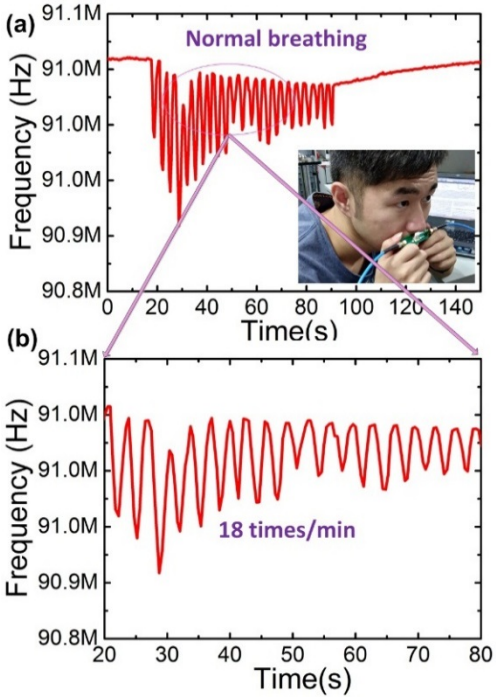

Figure 9. Resonant frequency shift of the graphene based SAW sensor at breathing for normal state, with wavelength of 40 μm.

4. Conclusion

In summary, we have demonstrated SAW resonators using graphene as the virtually massless IDT electrodes and the effects of graphene electrode on the performance of the SAW

devices were investigated and compared with theoretical analysis. The results showed that 4-layers graphene with the sheet resistance less than 77.6 Ω/sq. and 80 pairs of IDTs are needed to obtain good performance of SAW devices, and the graphene electrodes should have an optimal ratio of aperture/wavelength of 5. Base on this, the graphene based SAW devices with wavelength of 24 μm, resonance 154 MHz, transmission signal amplitude of 30 dB and K^2 of 3.78% were obtained, and has been successfully used in human breathing monitoring.

Supplementary Material

Supplementary material Shows the details of FEM/BEM theoretical analysis.

Acknowledgements

This work was supported by the National Natural Science Foundation of China (No. 51605485), National University of Defense Technology Research Project (No. ZK16-03-11) and UK Engineering and Physical Sciences Research Council (EPSRC, EP/P018998/1).

References

[1] Lee K, Wang W, Kim T and Yang S 2007 *J. Micromech. Microeng.* **17** 515
[2] Fachberger R and Erlacher A 2010 *Procedia Eng.* **5** 224-7
[3] Yeo L Y and Friend J R 2014 *Annu. Rev. Fluid Mech.* **46** 379-406
[4] Fu Y Q, Li Y, Zhao C, Placido F and Walton A J 2012 *Appl. Phys. Lett.* **101** 647
[5] Ding X et al 2013 *Lab Chip* **13** 3626-49
[6] Fu Y Q, Luo J K, Du X Y, Flewitt A J, Li Y, Markx G H, Walton A J and Milne W I 2010 *Sens. Actuators B* **143** 606-19
[7] Fu Y Q et al 2017 *Prog. Mater. Sci.* **89** 31
[8] Zhou J, Pang H F, Garcia-Gancedo L, Iborra E, Clement M, Miguel-Ramos M D, Jin H, Luo J K, Smith S and Dong S R 2015 *Microfluid. Nanofluid.* **18** 537-48
[9] Guo Y J, Lv H B, Li Y F, He X L, Zhou J, Luo J K, Zu X T, Walton A J and Fu Y Q 2014 *J. Appl. Phys.* **116** 1458
[10] Mayorov A, Hunter N, Muchenje W, Wood C, Rosamond M, Linfield E, Davies A and Cunningham J 2014 *Appl. Phys. Lett.* **104** 083509
[11] Leong A, Swamy V and Ramakrishnan N 2017 *Jpn. J. Appl. Phys.* **56** 024301
[12] Jr M M D L, Seidel W, Kostial H and Santos P V 2004 *J. Appl. Phys.* **96** 3494-500
[13] Huang X, Zeng Z, Fan Z, Liu J and Zhang H 2012 *Adv. Mater.* **24** 5979
[14] Knapp M D, Hoffmann R, Lebedev V, Cimalla V and Ambacher O 2018 *Nanotechnology* **29** 105302
[15] Zhou J, Xiao D B, Song Z X, Zhuo M, Wu X Z 2018 *IEEE Micro Electro Mechanical Systems* **79**
[16] Bae S, Kim H, Lee Y, Xu X, Park J S, Zheng Y, Balakrishnan J, Lei T, Kim H R and Song Y I 2010 *Nat. Nanotechnol.* **5** 574
[17] Wang Y, Tong S W, Xu X F, Ozyilmaz B and Loh K P 2011 *Adv. Mater.* **23** 1514-8
[18] Wang Y Y, Ni Z H, and Shen Z X, 2008, Appl. phys. Lett., **92**, 043121
[19] Ventura P, Hode J M and Lopes B 1995 *Ultrasonics Symposium* **1** 257-62
[20] Plessky V P and Thorvaldsson T 1995 *IEEE Trans. Ultrason. Ferroelectr. Freq. Control* **42** 280-93
[21] Smith W R, Gerard H M, Collins J H, Reeder T M and Shaw H J 1969 *IEEE Trans. Microw. Theory Tech.* **17** 856-64
[22] Lu X, Chen Z., Huang X, Chen T, Chen P 2013 *Piezoelectrics & Acoustooptics* **31** 4
[23] Vellekoop M J 1997 *Sens. Actuators A* **63** 79
[24] Yamada T, Hayamizu Y, Yamamoto Y, Yomogida Y, Izadinajafabadi A, Futaba D N and Hata K 2011 *Nat. Nanotechnol.* **6** 296
[25] Jin H, Tao X, Dong S, Qin Y, Yu L, Luo J and Deen M J 2017 *J. Micromech. Microeng.* **27**, 115006